UNIVERSITY OF PARDUBICE

FACULTY OF CHEMICAL TECHNOLOGY

Department of General and Inorganic Chemistry

Kateřina Čermák Šraitrová

Intrinsic defects and doping of SnSe

Theses of Doctoral Dissertation

Pardubice 2021

Study program: **Chemistry and Technology of Materials**

Study field: **Chemistry and Technology of Inorganic Materials**

Author: **Ing. Kateřina Čermák Šraitrová**

Supervisor: **prof. Ing. Čestmír Drašar, Dr**.

Year of the defence: 2021

References

ČERMÁK ŠRAITROVÁ, Kateřina. *Intrinsic defects and doping of SnSe*. Pardubice, 2021. 119 pages. Dissertation thesis (Ph.D.). University of Pardubice, Faculty of Chemical Technology, Department of General and Inorganic Chemistry. Supervisor Prof. Ing. Čestmír Drašar, Dr.

Abstract

SnSe is semiconductor with marked thermoelectric properties. In view of its 2D nature it could be interesting also in terms of spintronics. Properties of SnSe are strongly connected with the concentration of intrinsic defects (vacancies) and with the interaction of intrinsic defects with the dopants. I investigated the temperature dependence (1073-473 K) of equilibrium concentration of vacancies in stoichiometric SnSe and further the interaction of dopant (As) with defect structure of SnSe. I studied two compositional sets $SnSe_{1-x}As_x$ and $Sn_{1-x}As_xSe$. The materials were explored using positron annihilation, measurement of transport parameters and structural and chemical composition. The work reveals new fundamental findings in terms of point defects in SnSe and their interaction with doping species (As).

Abstrakt

SnSe je polovodič s výraznými termoelektrickými vlastnostmi, který však díky své 2D povaze může být zajímavý např. i z hlediska spintroniky. Vlastnosti SnSe jsou úzce svázány s koncentrací nativních defektů (vakancí) ale také jejich interakce s dopantem. Vyšetřovala jsem teplotní závislosti (1073-473 K) rovnovážné koncentrace vakancí ve stechiometrickém SnSe a dále také interakce dopantu (As) s defektní strukturou SnSe. Studovala jsem dvě dopovací řady $SnSe_{1-x}As_x$ a $Sn_{1-x}As_xSe$. Ke studiu jsem využila pozitronovou anihilaci, měření transportních parametrů, strukturní i chemickou analýzu. Práce přináší nové zásadní poznatky o nativních defektech ve struktuře SnSe, jejich závislosti na teplotě a jejich interakci s arsenem.

Keywords

Tin(II) selenide, SnSe, intrinsic defects, vacancies, doping

Klíčová slova

Selenid cínatý, SnSe, nativní defekty, vakance, dopování

Table of Contents

Introduction

Thermoelectric (TE) materials represent one of the alternatives for green energy and waste heat recovery. They can be also used as cooling devices without the use of freons. The TE efficiency of a material can be expressed in terms of the dimensionless figure of merit, ZT, where $ZT = S^2\sigma T/\kappa$ [1]. In this formula, S, σ, T, and κ are the Seebeck coefficient, electrical conductivity, absolute temperature, and thermal conductivity of the material, respectively. These parameters are interconnected via band structure and Wiedemann-Franz law.

Recently, Zhao et al. [2] published record ZT values ZT = 2.6 at 923 K along b axis of SnSe single crystal. Gradually, several problems with SnSe arised. First of them is the discrepancy between single crystal and polycrystalline results. While SnSe single crystals have excellent TE properties at elevated temperatures [2], polycrystalline SnSe yields mediocre [3]. One of the reasons is that single crystals reach much lower values of thermal conductivity in comparison with polycrystals. Furthermore, long-term stability of both doped and undoped samples seems to be questionable [4].

Recently, more attention has been given to intrinsic defects [5-8]. These defects, namely tin vacancies, seem to play a very important role in excellent properties of SnSe at elevated temperatures [5,9]. Together with tin vacancies selenium interstitials seem to play an important role in transport properties. Their large concentration might be responsible for extremely low thermal conductivity of SnSe [7]. The equilibrium concentration of interstitial defects is generally a function of temperature. Data about the thermal stability and equilibrium stoichiometry as a function of temperature are missing in the literature from both experimental and theoretical point of view.

Many elements and compounds have been studied as potential dopants for improving the TE properties of SnSe with mixed results.

In the first part of presented dissertation we investigated the development of intrinsic defects (vacancies) in SnSe single crystals as a function of annealing temperature. For this purpose, we prepared a series of stoichiometric single crystals annealed for long time and quenched at temperatures between 1073 K and 473 K. Second part deals with ambivalent arsenic doping study. With the aim to explore the interaction of doping species with intrinsic defects, we prepared two series $SnSe_{1-x}As_x$ and $Sn_{1-x}As_xSe$ in both polycrystalline and single crystalline form.

Prepared materials were characterized by powder X-ray diffraction (PXRD). Single crystalline samples were oriented using electron back scatter diffraction (EBDS). Arsenic content in doped single crystals was determined using inductively coupled plasma optical emission spectrometry (ICP-OES). Doped single crystals were also inspected with high resolution X-ray diffraction (HRXRD).

Transport properties as electrical conductivity σ, Hall coefficient R_H and Seebeck coefficient α were measured on all single crystalline and polycrystalline samples. For polycrystalline samples thermal conductivity κ was also estimated.

Both undoped and doped single crystals were investigated by means of positron annihilation spectroscopy (PAS).

This work brings several important results concerning intrinsic defects in SnSe, their temperature dependence and their interaction with doping atoms.

1 SnSe as thermoelectric material

Tin selenide (SnSe) is a very promising thermoelectric material, that belongs among the IV-VI compounds. At room temperature (α phase) it is characterised by a complicated orthorhombic structure with *Pnma* symmetry. This complicated structure is one of the prerequisites of very low thermal conductivity of SnSe. Above ~ 810 K it changes (β phase) to the *Cmcm* symmetry [10]. Neutron diffraction study of SnSe single crystals showed, that at ~ 810 K it undergoes so called *displacive phase transition* [10,11].

Layered *Pnma* structure results in anisotropic properties of SnSe. While properties measured along *b* and *c* axis vary only negligibly, properties along the *a* axis are significantly lower. As a result, in majority of works presented data are measured along *b* axis [2].

The only parameter, that is practically constant for all three axes, is Seebeck coefficient. Most discussed parameter is thermal conductivity. While single crystals along the *b* axis reach values about ~ 0.7 $Wm^{-1}K^{-1}$ [2], polycrystalline samples reach values about ~ 1-1.2 $Wm^{-1}K^{-1}$ [3]. According to the nature of polycrystalline samples it should be the other way around.

Electrical conductivity grows rather rapidly above ~ 600 K. This increase is ascribed to the formation of tin vacancies with a formation energy of 0.67 eV [5]. We are left with the question of how to preserve high concentration of tin vacancies at lower temperature. Equlibrium drives a tin understoichiometric composition towards the formation of the secondary phase $SnSe_2$ instead of the formation of tin vacancies at all temperatures [12].

Together with tin vacancies, another intrinsic defect, interstitial Se seems to play an important role in transport properties. An extra-large concentration of these defect might be responsible for extremely low thermal conductivity [7]. Such intrinsic defects would provide excellent TE performance even at lower temperatures if induced artificially. However, it is not clear how to induce these defects in the lower temperature range or stabilize them upon cycling. Again, excess Se should react with SnSe and produce $SnSe_2$ [12].

Based on the excellent TE properties of undoped SnSe single crystals it is general effort to further improve these properties. One of the ways is doping, i.e. introducing of the foreign atoms into the structure.

Many elements and compounds have been studied as potential dopants for improving of the TE properties of SnSe with mixed results. The majority of doping studies deal with *p*-type doping. To date, dopants such as Ag [4], alkali metals [13], Tl [14] and Cd [15] have been studied. According to band studies [5,16], n-type SnSe should have superior TE properties in comparison with p-type SnSe. However, it seems to be difficult to prepare n-type SnSe. Only a few studies deal with n-type doping, e.g., material doped with Bi [17] of Br [18]. So far, a suitable and stable dopant for shifting the efficiency maximum to a lower temperature region has not been found.

2 Experimental

For the investigation of the development of intrinsic vacancies in SnSe a series of stoichiometric single crystals quenched from annealing temperatures (ATs) between 1073 K and 473 K was prepared. Stoichiometric SnSe single crystals were grown using the free melt crystallization (FMC) method. A stoichiometric mixture of 5N Sn and Se elements was loaded into quartz ampoules and sealed under vacuum ($p < 10^{-3}$ Pa). Then, the ampoules were heated to 1223 K at a rate of 1.7 K/min and kept at this temperature for 6 h. Crystal growth involved cooling at a rate of 0.1 K/min to 1073 K. The crystals were annealed at this temperature for 168 h. Subsequently, one of the ampoules was quenched in air, and the rest of them were further cooled (0.1 K/min) to 973 K. The ampoules were kept at this temperature for 168 h, and one of them was quenched in air. This process was repeated using lower and lower temperatures until a temperature of 473 K was reached. Thus, a series of samples quenched from annealing temperatures (ATs) of 1073, 973, 873, 793, 773, 673, 623, 603, 573, and 473 K was prepared. These temperatures are used as labels for each sample (e.g., 473 K AT).

For the investigation of the influence of ambivalent dopant As on the SnSe structure, at first two polycrystalline series were prepared. Polycrystalline samples with the composition $Sn_{1-x}As_xSe$ (x = 0-0.1) and $SnSe_{1-x}As_x$ (x = 0-0.08) were synthesized from Sn and Se elements (of 5N purity) and compound SnAs (synthesized) in desired stoichiometry. Evacuated ampoules were heated to 1223 K over 10 hours, maintained at this temperature for 6 hours, and then cooled down to room temperature by switching off the furnace. The products were powdered for 1 min in a vibrating mill under hexane and identified by X-ray diffraction (XRD). The samples for physical measurements were hot-pressed at 713 K and 70 MPa for 1 hour. Compact disc-shaped samples (with diameter 12 mm and thickness cca 2 mm) and rectangular samples (with dimensions $10\times3.5\times10$ mm^3 and 10 mm in the direction of pressing) reached ≥95 % of theoretical (X-ray) densities of the prepared compounds.

For detailed investigation of the interaction of As with SnSe structure and its intrinsic defects, As doped single crystals were prepared. Evacuated ampoules containing elemental Sn and Se (of 5N purity) and compound SnAs (synthesized) at the desired stoichiometry were heated (1.7 K/min) in a furnace up to 1223 K and remained at this temperature for 6 hours followed by slow cooling (0.1 K/min) to 293 K. Using this procedure, we obtained two sets of As-doped SnSe: $SnSe_{1-x}As_x$ (x = 0–0.01), and $Sn_{1-x}As_xSe$ (x = 0–0.01).

For the investigation of the influence of non-stoichiometry on the development of intrinsic defects in SnSe, a series of non-stoichiometric $Sn_{2-y}Se_y$ (y = 0.99 – 1.01) single crystals was also prepared. These crystals were prepared the same way as arsenic doped single crystals.

For further measurements, single crystalline specimens with dimensions of $10\times3\times0{,}1$ mm^3 were cut out of the ingots.

X-ray diffraction (PXRD) patterns (Cu Kα, λ = 1.5418 Å) were recorded for all (powdered) samples using a D8 Advance diffractometer (Bruker AXES, Germany) with a Bragg-Brentano Θ − Θ goniometer (radius 217.5 mm) equipped with a Ni-beta filter and a LynxEye detector. Scans were performed at room temperature in the range from 10° to 90° (2Θ) in 0.01° steps with a counting time of 2 s per step. The lattice parameters were refined using the Le Bail method as implemented in the program FULLPROF [19].

High-resolution X-ray diffraction (HRXRD) was used to closer inspection of the arsenic doped single crystals layered structure. For this purpose, RIGAKU Smartlab diffractometer equipped with a rotating Cu anode (45 kV, 200 mA) and a 2x220Ge crystal monochromator, and the diffracted intensity was measured by a one-dimensional detector was used.

Orientation of single crystalline samples was performed using electron backscatter diffraction (EBSD) on JEOL 733 equipped with an energy-dispersive X-ray analysis EBSD detector. EBSD data were analysed with TSL OIM software.

The elemental analysis of arsenic doped single crystals was carried out with the sequential, radially viewed ICP (Inductively Coupled Plasma) atomic emission spectrometer INTEGRA 6000 (GBC, Dandenong Australia), equipped with the concentric nebulizer and the glass cyclonic spray chamber (both Glass Expansion, Australia). The analytical line 193.696 nm was used. For an instrumental calibration, calibration standards containing 10 – 5 – 1 - 0.5 - 0.1 $mg.L^{-1}$ of As were used. The calibration standards were prepared using commercially available stock standard solution of As containing 1 g/dm^3 (SCP, Baie D'Urfé, Canada). The instrumental limit of detection (the concentration equal to three times standard deviation in the place of background correction) was 0.5 $mg.L^{-1}$, the repeatability of the ICP OES measurement is usually in the range 1 – 2 %.

The transport parameters measured on the single crystalline samples include the electrical conductivity σ ($i||b$), the Hall coefficient R_H ($i||b$; $B||a$), and the Seebeck coefficient α ($\Delta T||b$). These parameters were measured over a temperature range from 80 to 470 K. A conductive graphite adhesive was used to attach the current and voltage leads. The Hall effect and electrical conductivity were examined using a lock-in nanovoltmeter with a 29-Hz excitation and a static magnetic field of 0.6 T. The Seebeck coefficient was determined using the longitudinal steady-state technique with a temperature difference ranging from 3 to 3.5 K. The thermal gradients were measured with the aid of fine copper-constantan thermocouples.

The transport parameters of the polycrystalline samples were measured over a temperature range from 300 to 725 K. Electrical conductivity σ was measured with four-probe method using lock-in amplifier (model 5209; EG&C, Princeton; USA). The Seebeck coefficient α was determined by means of a static dc method on disc-shaped samples. The temperature gradient between two points was measured with two shielded K-type thermocouples pressed against the sample surface. A potential difference dU corresponding to the gradient dT was measured across the same legs of both attached thermocouples. The absolute Seebeck coefficient was determined from the slope dU/dT.

The thermal diffusivity k of the polycrystalline samples was measured from 300 to 725 K on round hot-pressed samples using the respective instrument (model LFA 457; Netzsch-Gerätebau, Selb, Germany). The thermal conductivity κ was subsequently calculated using the relation: $\kappa = k \times c_p \times \rho$, where ρ is the experimental density and c_p the heat capacity. Inconel was used as the heat capacity standard. We used an average $c_p = f(T)$ based on c_p-measurements of all the samples of the $Sn_{1-x}As_xSe$ and $SnSe_{1-x}As_x$ series. We assume that rather low content of As in the host compound has only a negligible effect on the heat capacity of host matrix.

Single crystals were characterized using positron annihilation spectroscopy (PAS). A carrier-free ^{22}Na radioisotope with an activity of ≈ 1 MBq deposited on a 2-μm-thick Mylar foil was used as a positron source. Two complementary PAS techniques were

employed: positron lifetime (LT) spectroscopy [20], which enables the identification of defects and the determination of their concentrations, and coincidence Doppler broadening (CDB) [21], which provides information about the local chemical environment of the defects. PAS measurements were carried out at room temperature. A digital spectrometer described in Ref. [22] was employed for the LT measurements. The spectrometer has a time resolution of 145 ps (full width at half maximum of the resolution function). The LT spectra, which always contained at least 10^7 positron annihilation events, were decomposed using a maximum-likelihood code [23]. The CDB studies were carried out using a digital spectrometer [24] equipped with two high-purity Ge detectors and characterized by an energy resolution of 0.9 keV at the annihilation line of 511 keV and a peak-to-background ratio higher than 10^5. The results of the CDB measurements are presented as ratio curves with respect to Al (99.9999%).

3 SnSe single crystals annealed and quenched at different temperatures

3.1 Powder X-ray diffraction (PXRD)

No foreign phases were observed at any AT. An example of the PXRD pattern is depicted in Fig. 1. The unit-cell volume as a function of AT is shown in the inset. All the lattice parameters (*a, b, c*) show similar behavior. The evolution of the unit-cell volume (UCV) with AT reflects the AT dependence of the concentration of intrinsic defects as will be discussed in section 3.2.

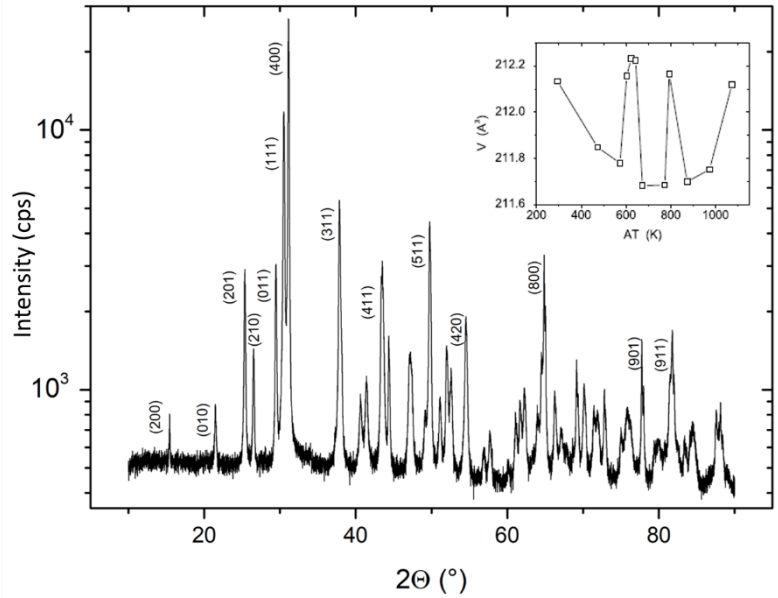

Fig. 1. A typical PXRD pattern of a powdered SnSe single crystal. No traces of foreign phases are detectable. The inset documents the variation of UCV with AT. The maximum deviation of the UCV is ± 0.1 A^3.

3.2 Positron annihilation spectroscopy (PAS)

The lifetimes for the various positron states obtained from *ab initio* calculations are listed in Table I. The calculated bulk positron lifetime, i.e., the lifetime of free positrons delocalized in a perfect (defect-free) lattice of the *Pnma* phase of SnSe, is τ_B = 217 ps.

Figure 2 shows the development of the mean positron lifetime with annealing temperature. The dashed lines in Fig. 2 indicate the calculated lifetimes for various positron states. With an AT increasing above 300 K, τ_{mean} first slightly decreases towards the bulk value and shows a minimum at approximately 500 K. Thus, the lowest concentration of defects occurs at approximately 500 K. Above 600 K, the mean positron lifetime steeply increases even above the values calculated for V_{Se} and V_{Sn}, indicating a dramatic increase in the concentration of defects and the introduction of defects with a larger open volume than monovacancies.

Table I. The bulk positron lifetime and the lifetimes of positrons trapped at various point defects obtained from ab initio calculations.

Positron state	τ (ps)
Bulk	217
V_{Sn}	308
V_{Se}	279
V_{Sn} + V_{Se}	358
V_{Sn} + 2 V_{Se}	396
V_{Sn} + 3 V_{Se}	431

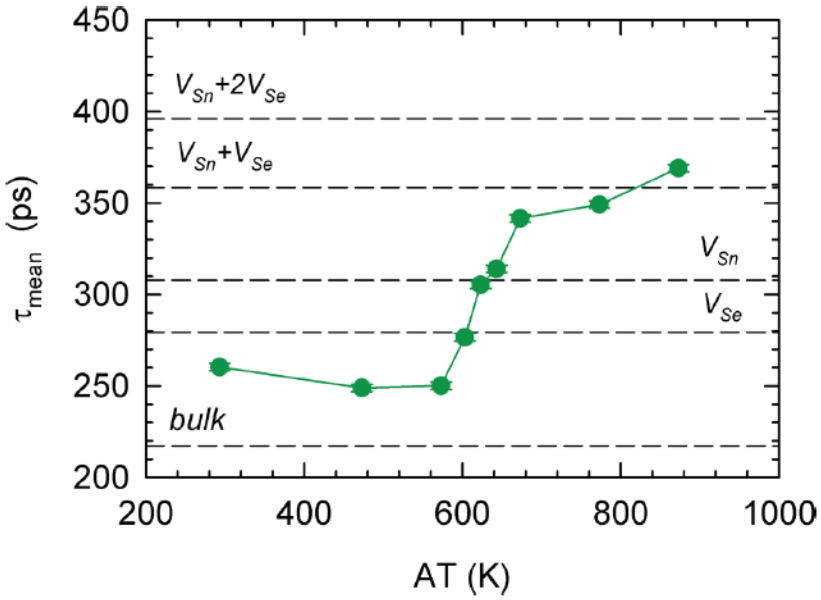

Fig. 2. The development of the mean positron lifetime τ_{mean} as a function of AT. The dashed lines show the calculated positron lifetimes for a perfect SnSe lattice (bulk) and for various types of defects.

Figure 3 shows the development of the lifetimes τ_i of the exponential components resolved in the LT spectra with AT. The dashed lines in the figure again indicate the lifetimes calculated for various kinds of defects.

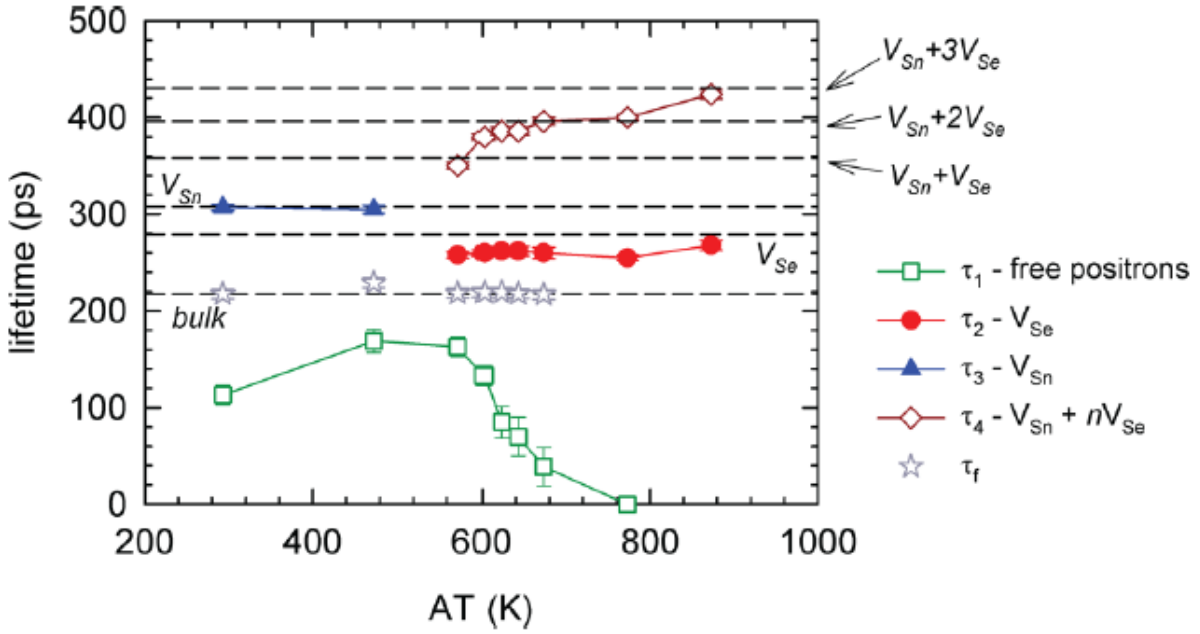

Fig. 3. The development of the lifetimes τ_i of the exponential components resolved in the LT spectra as a function of AT. The dashed lines show calculated lifetimes for various positron states.

The development of the corresponding intensities I_i of the components resolved in the LT spectra is plotted in Fig. 4 as a function of AT. From the intensity behavior in Fig. 4, it becomes clear that Sn vacancy represents the dominant type of defect at an AT ≈ 300 K. With increasing AT, the concentration of V_{Sn} rapidly decreases, which leads to a pronounced drop in I_3. Above 600 K, the nature of the defects changes: the Sn-vacancy component cannot be resolved in LT spectra anymore, but two other components appear. Namely, Se vacancies and vacancy clusters $V_{Sn} + nV_{Se}$ where n varies between 1 and 3. From the development of the intensities in Fig. 4, one can conclude that the concentration of V_{Se} and $V_{Sn} + nV_{Se}$ increases with AT in the temperature range 600–800 K and becomes saturated above 800 K. Hence, V_{Se} and $V_{Sn} + nV_{Se}$ represent the dominant type of defect at elevated temperatures (AT > 600 K).

The concentrations of the point defects [V_{Sn}], [V_{Se}], and [$V_{Sn} + nV_{Se}$] determined from the LT data are plotted in Fig. 5 as a function of AT. From inspection of the figure, it becomes clear that [V_{Sn}] decreases with AT and diminishes at 600 K. Above this temperature, V_{Se} and $V_{Sn} + nV_{Se}$ appear, and their concentrations [V_{Se}] and [$V_{Sn} + nV_{Se}$] strongly increase with AT.

The experimental CDB ratio curves for SnSe SCs are plotted in Fig. 6. The CDB ratio curves for reference samples of pure Sn and Se are plotted in the figure as well. The shapes of the high-momentum parts of the CDB ratio curve for pure Sn and Se are in good qualitative agreement with the calculated Sn and Se contributions. From inspection of Fig. 6, one can conclude that the CDB ratio curves for SnSe SCs for AT < 600 K exhibit similar features, namely a peak at $p \approx 9\times10^{-3}\, m_0c$ followed by a broad peak at higher momenta (~ 20×10−3 m_0c). The CDB curve for AT = 473 K is only vertically shifted up with respect to the curve for AT = 293 K. This indicates that for AT < 600 K positrons were annihilated in similar chemical environment, i.e., the

fraction of positrons annihilated in the vicinity of Sn and Se ions is comparable. In contrast, for AT ≥ 600 K the shape of the CDB curves significantly changes, indicating a change in the dominant type of defect. The calculated CDB ratio curves for various defects in SnSe are compared in Fig. 7.

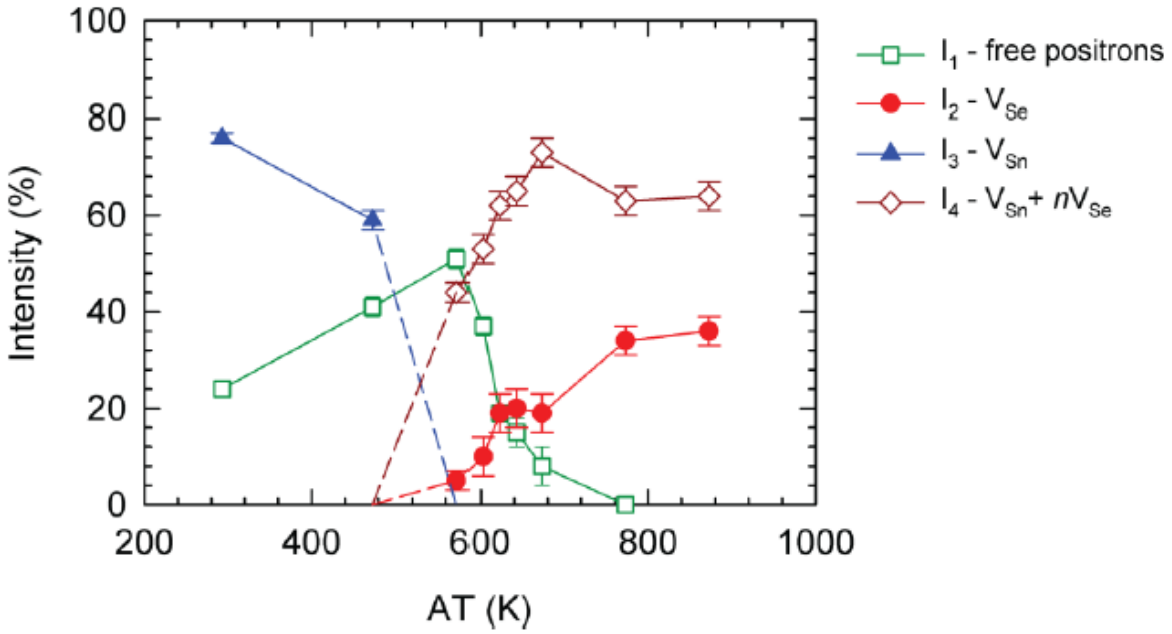

Fig. 4. The development of the relative intensities I_i of the exponential components resolved in the LT spectra as a function of AT. Dashed lines show extrapolation to zero intensity in case where the corresponding component could not be resolved in the spectrum.

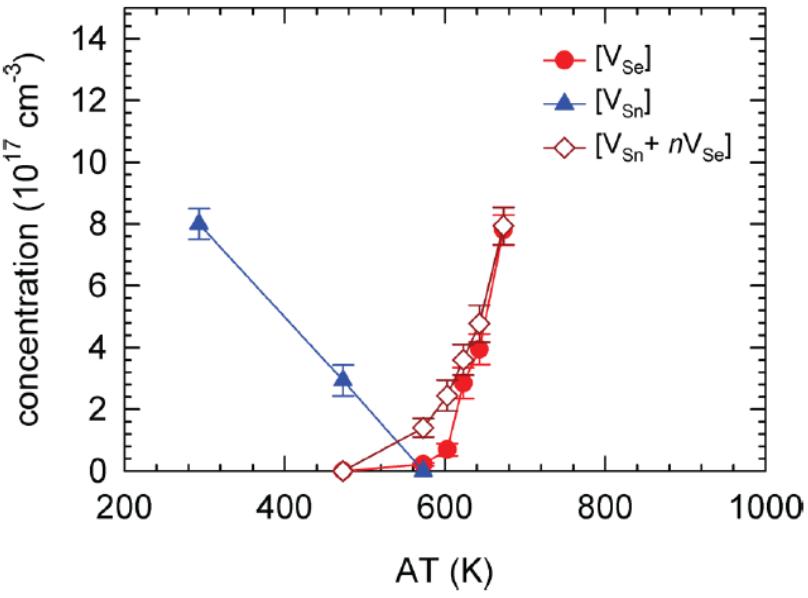

Fig. 5. The development of the concentrations of point defects detected by LT spectroscopy in SnSe SCs plotted as a function of AT.

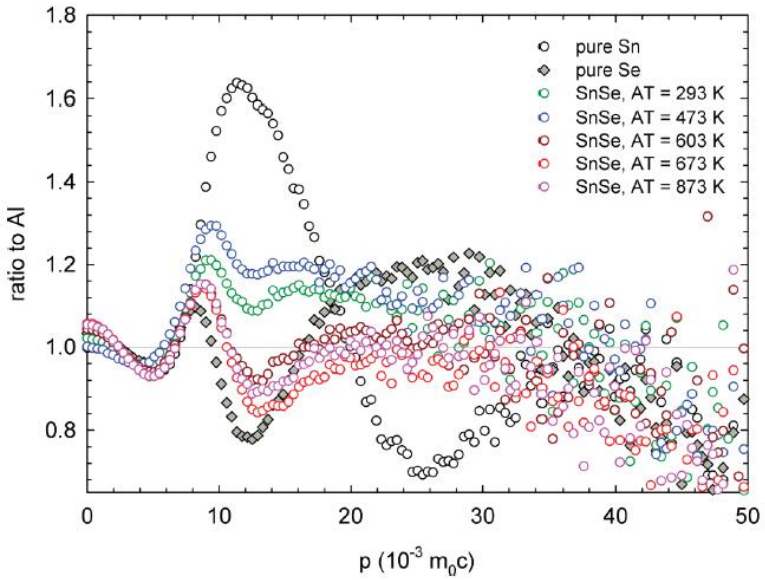

Fig. 6. Experimental CDB ratio curves (related to well-annealed pure Al) for SnSe SCs. The ratio curves for reference samples of pure Sn and Se are plotted in the figure as well.

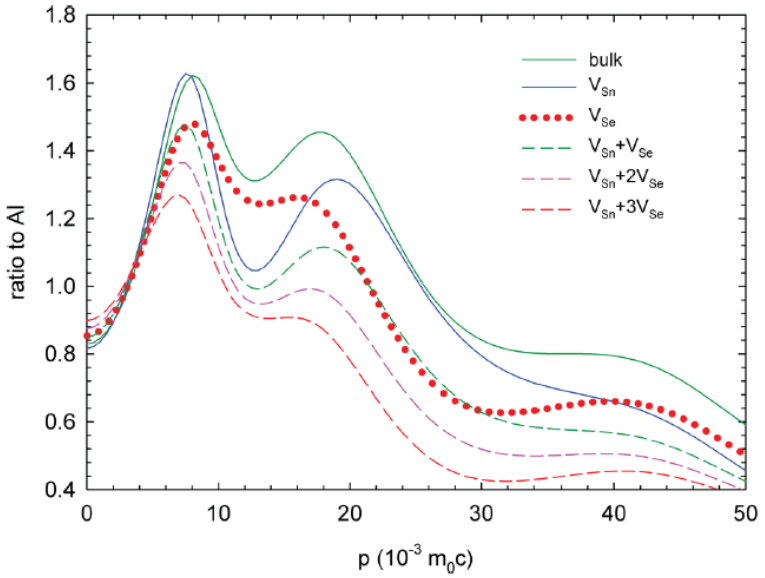

Fig. 7. Calculated CDB ratio curves (related to Al) for a perfect SnSe crystal and various point defects in SnSe.

Comparing Figs. 6 and 7, one can conclude that there is relatively good qualitative similarity between the CDB curves measured for SnSe SCs for AT < 600 K and the calculated CDB curve for V_{Sn}. This is in accordance with V_{Sn} representing the dominating type of defect for AT < 600 K. An enhancement of the experimental CDB curve in the highmomentum range caused by an increase in AT from 293 to 473 K corresponds well to a decrease in V_{Sn} concentration, i.e., a shift of the CDB ratio curve towards the curve for the bulk. For AT = 603 K and higher temperatures, the experimental CDB ratio curves drop in the high-momentum range (Fig. 6). This indicates the introduction of defects with a larger open volume than the open volume of V_{Sn}, which is consistent with the creation of $V_{Sn} + nV_{Se}$ clusters, cf. Fig. 5. Indeed, the shape of the experimental CDB ratio curves for AT ≥ 600 K is in good qualitative

agreement with the calculated curves for the $V_{Sn} + nV_{Se}$ clusters. The drop in the experimental CDB curves in the high-momentum range is more pronounced when AT increases from 603 to 873 K (see Fig. 6). This is in accordance with the increasing concentration of $V_{Sn} + nV_{Se}$ clusters. Hence, the CDB investigations support the picture that the Sn vacancy represents the dominating type of defect at AT < 600 K, while at higher temperatures (AT ≥ 600 K) the dominating defect changes to V_{Se} and $V_{Sn} + nV_{Se}$.

3.3 Transport properties

The Hall free carrier (FC) concentration *h* as a function of AT is shown in Fig. 8. We used the simplified formula $h = 1/R_H e$, with R_H being the Hall coefficient. The lowest hole concentration is achieved by annealing in the range from 473 to 573 K. This is in accordance with the lowest concentration of vacancies measured by PAS. We observe a steep increase in the hole concentration for sample 673 K AT passing from 300 to 400 K, which indicates thermal excitations.

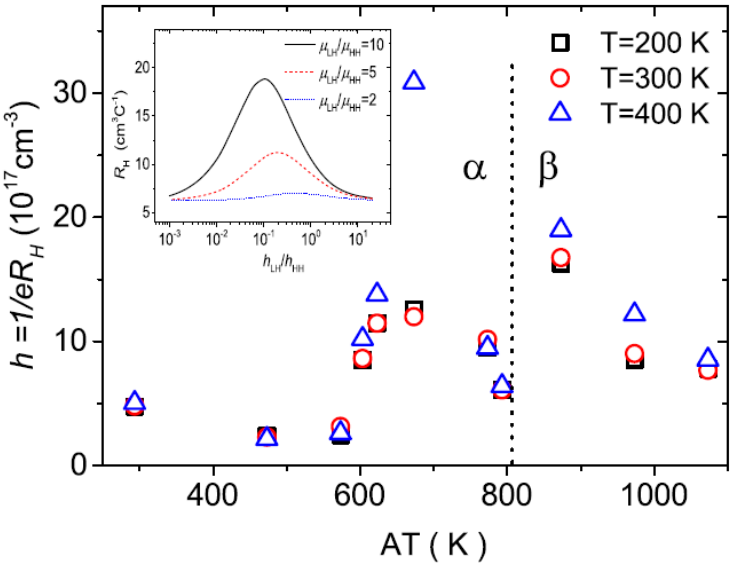

Fig 8. Hall concentration h of holes of SnSe as a function of AT for three temperatures. Note the significant increase in the hole concentration between 300 and 400 K for 673 K AT, which is indicative of thermal excitation. The dotted line represents the α→β transition temperature (≈810 K) of SnSe. The inset documents the eventual impact of heavy holes (HH) if combined with light holes (LH) in terms of carrier mobility. The curves are calculated using $R_H = \frac{1}{|e|}\frac{(h_{HH}\mu_{HH}^2+h_{LH}\mu_{LH}^2)}{(h_{HH}\mu_{HH}+h_{LH}\mu_{LH})^2}$ *where h and μ are the respective hole concentration and mobility.*

The Hall mobility μ_H (Fig. 9) is comparable in magnitude with the data published in Ref. [17]. In accordance with the PAS results, the mobility of FC increases with a decreasing concentration of V_{Sn} and peaks around AT ≈ 600 K, i.e., close to the temperature where the lowest concentration of defects is found. An interesting transient drop in FC mobility (and partially in the PF) appears at an AT of approximately 773 K (Fig. 9). This suggests that the concentration of defects (disorder) is higher at 773 than at 793 K, which is a temperature on the verge of the *α→β* transformation. Indeed, the

concentration of $V_{Sn} + nV_{Se}$ clusters is lower at 793 than at 773 K according to PAS (see a drop of I_4 in Fig. 5). On the other hand, this can suggest that the transition temperature is lower than 800 K, as reported in Ref. [25].

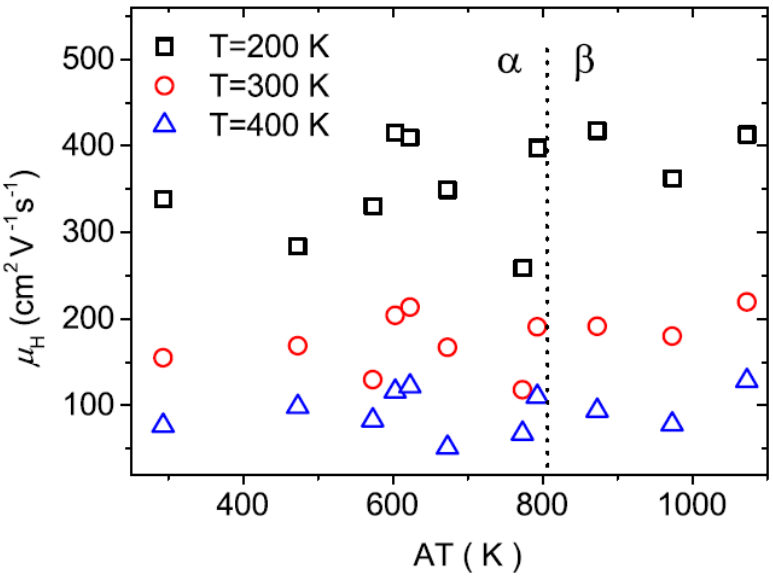

Fig 9. Hall mobility μ_H of SnSe as a function of AT for three temperatures. The dotted line represents the α→β transition temperature (≈ 810 K) of SnSe.

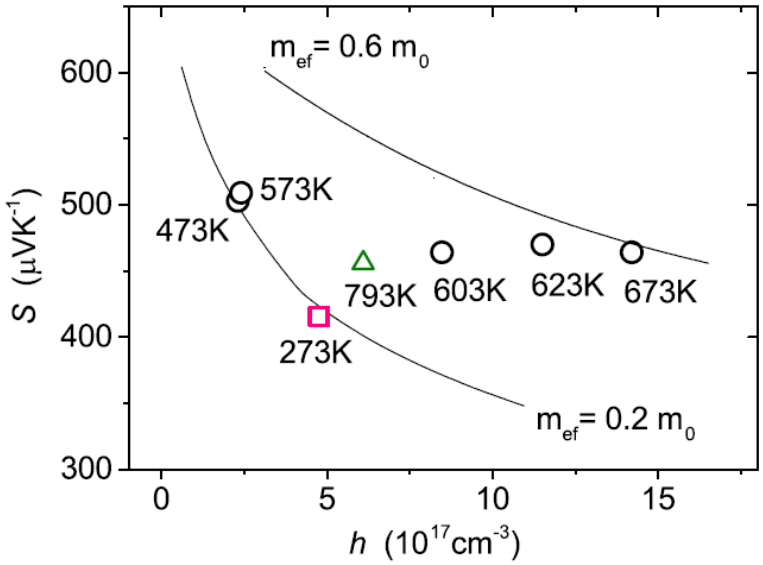

Fig 10. The Seebeck coefficient S as a function of the Hall concentration of holes (Pisarenko plot) for various ATs (not shown are the samples annealed above the α→β transition temperature ≈ 810 K). The solid lines are fits using a single parabolic model assuming scattering of FCs by acoustic phonons. The sample annealed at 793 K (green triangle) is on the verge of the α→β transition. The red square represents the standard (nonannealed) sample. The values were measured at T = 200 K.

Figure 10 shows the Seebeck coefficient as a function of the hole concentration (Pisarenko plot) for various ATs. The solid lines are fits to a single parabolic model assuming scattering of FCs by acoustic phonons [26]. A marked virtual increase in the

density of states (DOS) effective mass of FC was observed when AT increased from 473 to 673 K. It is obvious that this violates the model. The results coincide with the outputs resulting from PAS and transport parameter analysis, i.e., with increasing defect concentration, which effectively leads to an increase in effective mass [6].

We propose idea that can help in explaining the extraordinary properties of SnSe: the extra energy filtering of the FCs by the V_{Se} defects or clusters of $V_{Sn} + nV_{Se}$ that mimic the increase in the DOS effective mass and the Seebeck coefficient. The virtual increase in the DOS effective mass can be induced by a shift of the scattering mechanism of the FCs towards a more energetically dependent one. An increasing concentration of V_{Se} and clusters might be the reason for this phenomenon in SnSe. In comparison with single vacancies, larger defects (clusters $V_{Sn} + nV_{Se}$) may provide more-pronounced energy filtering.

4 As doped SnSe polycrystals

The prepared hot-pressed samples showed anisotropic transport properties due to a preferential orientation of the layered SnSe crystallites and the uniaxial pressure of the hot-pressing process. That is why we have measured the transport properties of the pellets in the direction perpendicular to the pressing force.

The electrical conductivities σ of the $Sn_{1-x}As_xSe$ samples exhibit a semiconducting behavior and they are increasing with temperature in the whole temperature range. Even a very small addition of As causes a steep decrease in the electrical conductivity. The electrical conductivity of the $SnAs_xSe_{1-x}$ samples first increases to 520 K, then switches to metallic-like behavior up to about 650 K and, finally, again increases most likely due to the thermal carrier excitations over the fundamental gap [27].

For the $Sn_{1-x}As_xSe$ samples, even a small substitution of As for Sn causes a steep decrease of Seebeck coefficient values at lowest temperatures studied. That abrupt decrease with the decreasing temperature (even down to negative values for the samples with highest x) indicates that the samples approach an extrinsic regime and, eventually, switch from *p*-type to *n*-type. Thus, As-atom behaves like donor (although of very low efficiency). Similar steep decrease of Seebeck coefficient is observed also for the lowest values of x in the $SnSe_{1-x}As_x$ system at low temperatures. The Seebeck coefficient is positive for the samples of the higher x values and almost temperature-independent, resembling thus the behavior of the undoped SnSe sample.

In the Fig. 11, we present the Arrhenius plot to elucidate the observed variations in the transport properties. In the undoped sample ($x = 0$), the exponential increase of the electrical conductivity at higher temperatures corresponds to a thermal activation of free carriers. The V_{Sn}^{2-} act as a shallow acceptor with a very low activation energy, i.e. it forms acceptors levels very close to the valence band edge. Even a very small addition of As significantly suppresses the electrical conductivity of the compound. In our opinion, the As atoms substituting for Sn effectively prevent the formation of V_{Sn}^{2-} defects. Regarding the limited solubility of As in $Sn_{1-x}As_xSe$ samples we can offer following explanation. Part of the As atoms can substitute for Sn atoms, forming positively charged substitutional As_{Sn}^{+} defects compensated by the electrons. The suppression of the V_{Sn}^{2-} defects can reveal the existence of other positively charged point defects, contributing to the electrical transport. These could be selenium vacancies V_{Se}.

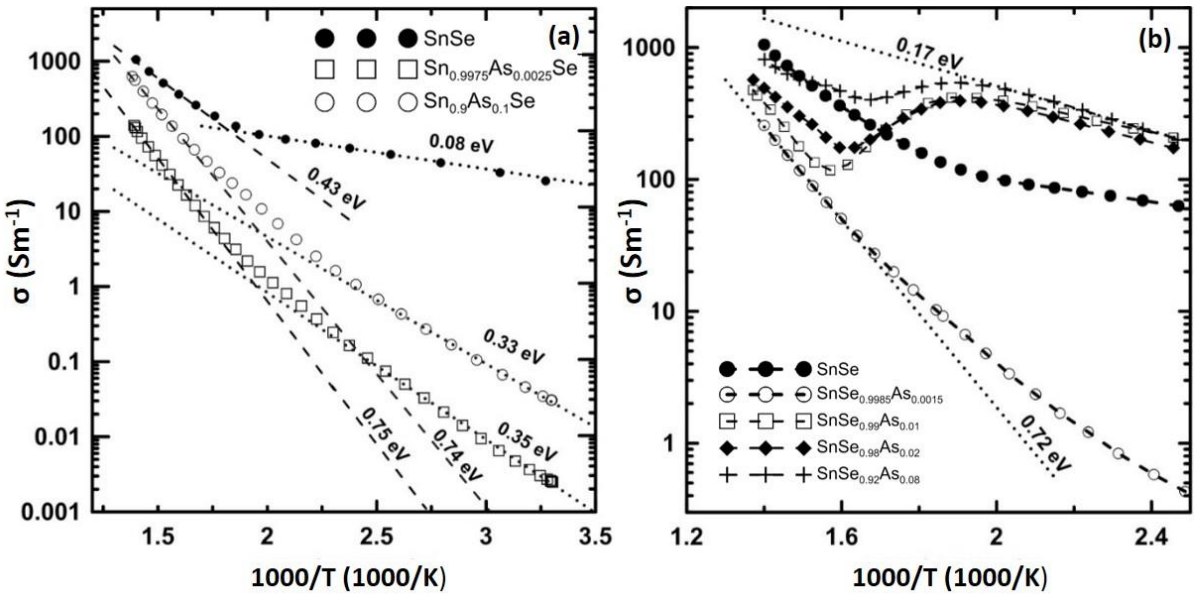

Fig. 11. Arrhenius plots of the electrical conductivities for selected $Sn_{1-x}As_xSe$ samples (a) and $SnAs_xSe_{1-x}$ samples (b).

For the system of nominal composition $SnSe_{1-x}As_x$, one can see again a very pronounced decrease of σ at the sample with the lowest As content. A qualitative resemblance of the temperature dependencies of both σ and S for this sample with those observed for the $Sn_{1-x}As_xSe$ leads us to the conclusion that even small substitution of the As atoms for Se atoms strongly suppresses the formation of V_{Sn}^{2-} in SnSe. The Arrhenius plot (Fig. 11*b*) reveals an activation energy of 0.17 eV for the samples with $x > 0.01$ in the lower temperature range. Such activation energy could be connected with the formation of As_{Se}^{-} defects introducing an acceptor level in the band gap of SnSe. Another explanation of the observed decrease of electrical conductivities at T~ 520 K can be related to a possible melting of tin. We should consider the presence of other phase in the $SnSe_{1-x}As_x$ compounds studied. SnAs impurity was observed in the samples with $x \geq 0.03$. In conclusion, we think that part of As enters the Se-sublattice forming As_{Se}^{-} and, at very low concentrations, this type of defects prevents the formation of tin vacancies as the major defects in the undoped SnSe. With the increased x, the As_{Se}^{-} defects become the main source of free holes responsible for the increase of electrical conductivity and for restoring the "pure" p-type character of the Seebeck coefficient. After reaching the solubility limit in $SnSe_{1-x}As_x$, As reacts with Sn to form SnAs.

The values of ZT in the case of $Sn_{1-x}As_xSe$ are for all doped samples lower than for undoped sample at low temperatures. With the increasing temperature, ZT values of the samples of lower x ($0.0025 \geq x \geq 0.01$) either quickly achieve the values for the undoped SnSe or even exceed it ($Sn_{0.9975}As_{0.0025}Se$). On the other hand, ZT values for most of the $SnAs_xSe_{1-x}$ samples significantly exceed the one for the undoped SnSe in the temperature range up to ca. 520 K, then, it suddenly fall below and being still lower than that of undoped SnSe at higher temperatures.

5 As doped SnSe single crystals

5.1 Sample composition

No foreign phases were observed at any composition. The unit cell volume varies with x for both sets. For the $SnAs_xSe_{1-x}$ single crystals, the changes in the a and b lattice parameters are small, while the c parameter and unit cell volume V increase significantly with x. This result indicates a higher As solubility compare to $Sn_{1-x}As_xSe$ set. For $Sn_{1-x}As_xSe$ set, the x-dependence of the lattice parameters is more complex. All the parameters peak for $x = 0.001$ and then decrease, as does the unit cell volume. These results are consistent with the results obtained from PAS and transport measurements (as will be discussed in 5.2 and 5.3) on both sets.

The preferential substitution of As for Se by comparing nominal and actual composition of samples was studied using ICP-OES method. The nominal and actual x are comparable in $SnAs_xSe_{1-x}$ set while the actual x is much lower than nominal x for $Sn_{1-x}As_xSe$ set. It indicates that As segregates within single crystal growth in $Sn_{1-x}As_xSe$

Closer inspection of the layered structure of the samples was carried out using HRXRD method. Next to the H00 peaks with even H, we observe the H00 peaks with odd H that are forbidden for the centrosymmetric SnSe structure. Although the peaks are very weak or even forbidden, the maximum of the envelope curve of the quasi forbidden peaks clearly moves to larger 2Θ with increasing As content. Although, we have no clear interpretation of this interesting effect at the moment, we anticipate that both the appearance and the shift is due to point defects. Importantly, the amount of $SnSe_2$ phase decreases with As concentration, especially for the $SnAs_xSe_{1-x}$, where no $SnSe_2$ lines appear for $x \geq 0.005$. From the widths of the $SnSe_2$ diffraction maxima, we estimate the mean vertical size of the $SnSe_2$ inclusions to be 10 ± 2 nm.

5.2 Positron annihilation spectroscopy (PAS)

Table II shows the LTs calculated for various positron states. Set of binary samples $Sn_{2-y}Se_y$ ($y = 0.99 – 1.01$) SCs with slightly varied stoichiometry have been studied for comparison in order to examine the effect of non-stoichiometry on the formation of point defects. Fig. 12 shows the development of the mean positron lifetime with the Se concentration y. SnSe exhibits the mean lifetime $\tau_{mean} \approx 260$ ps. For Se-rich samples ($y > 1$) τ_{mean} further increases, while in Sn-rich samples ($y < 1$) τ_{mean} decreases

Fig. 13 shows the trend of mean lifetime τ_{mean} with the content of As in the samples. The behaviour of τ_{mean} is markedly different for the $SnAs_xSe_{1-x}$ and $Sn_{1-x}As_xSe$ sets. The τ_{mean} decreases in $SnAs_xSe_{1-x}$ with increasing As concentration, approaching the defect-free bulk lifetime. This result indicates that the fraction of positrons annihilating in the trapped states gradually decreases with As content. The lowest concentration of defects occurs at approximately $x = 0.005$ for the $SnAs_xSe_{1-x}$ set, which reflects the off-stoichiometry of formally stoichiometric SnSe. In contrast, for $Sn_{1-x}As_xSe$, the mean lifetime increases to longer than 300 ps, indicating that annihilation occurs mostly in trapped states in open volume defects as the As content increases.

Table II. Life-times for various positron states in SnSe (Pnma) obtained from ab inito calculations.

Positron state	τ (ps)
Bulk	217
V_{Sn}	308
V_{Se}	279
$V_{Sn} + V_{Se}$	358
$V_{Sn}+2\ V_{Se}$	396
$V_{Sn} + 3\ V_{Se}$	431
$As_{Se} + V_{Sn}$	307
$As_{Se} + 2V_{Sn}$	315
$As_{Se} + 3V_{Sn}$	322
$As_{Se} + 4V_{Sn}$	331
$As_{Sn} + V_{Se}$	284
$As_{Sn} + 2V_{Se}$	301
$As_{Sn} + 3V_{Se}$	314
$V_{Sn} + As_{Se} + V_{Se}$	357

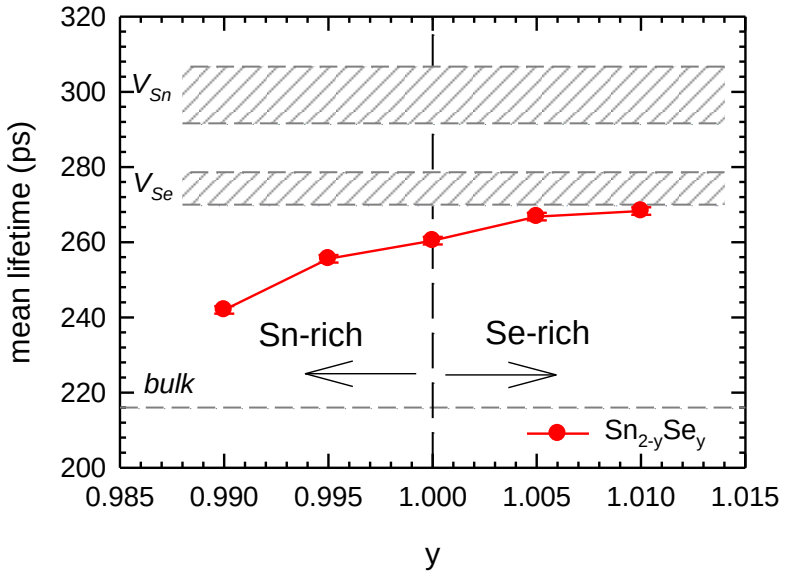

Fig 12. The development of the mean positron lifetime for binary $Sn_{2-y}Se_y$ SCs.

The concentrations of the point defects [V_{Sn}] (for $x = 0$) and [$V_{Sn} + nAs_{Se}$] ($SnAs_xSe_{1-x}$) and [$2V_{Sn}$] ($Sn_{1-x}As_xSe$) (for $x > 0$) determined from the LT data are plotted in Fig. 14. Inspection of Fig. 14 shows that the concentration of defects decreases with As content for the $SnAs_xSe_{1-x}$ set, while for the $Sn_{1-x}As_xSe$ set it increases. A closer inspection reveals that the concentration of defects decreases for both sets of samples for very low As concentration $x \leq 0.001$. Namely, we observe a drop in the concentration of V_{Sn} even for the $Sn_{1-x}As_xSe$), where the preferential substitution of As for Se drives

the crystal to Sn-poor composition. As discussed above, this result reflects that SnSe allows a small off-stoichiometry connected with rather high concentration of V_{Sn}. Hence, we conclude that although the As preferential substitution for Se generally increases the formation energy of V_{Sn} (the concentration of this defect should decrease), the shift in the stoichiometry towards cation poor composition induces the formation of cation vacancies in the $Sn_{1-x}As_xSe$. Hence, even in the $Sn_{1-x}As_xSe$, some fraction of As dopants substitute Se, which creates conditions favourable for the formation of V_{Sn}. Such formation of V_{Sn} is, however, observed for higher concentrations of As only. In fact, the $Sn_{1-x}As_xSe$ samples should be viewed as $Sn_{1-x}(As,Se)_{1+x}$. In terms of this notation, the preferential substitution of As for Se explains the increasing concentration of V_{Sn} in the $Sn_{1-x}As_xSe$, as stated above.

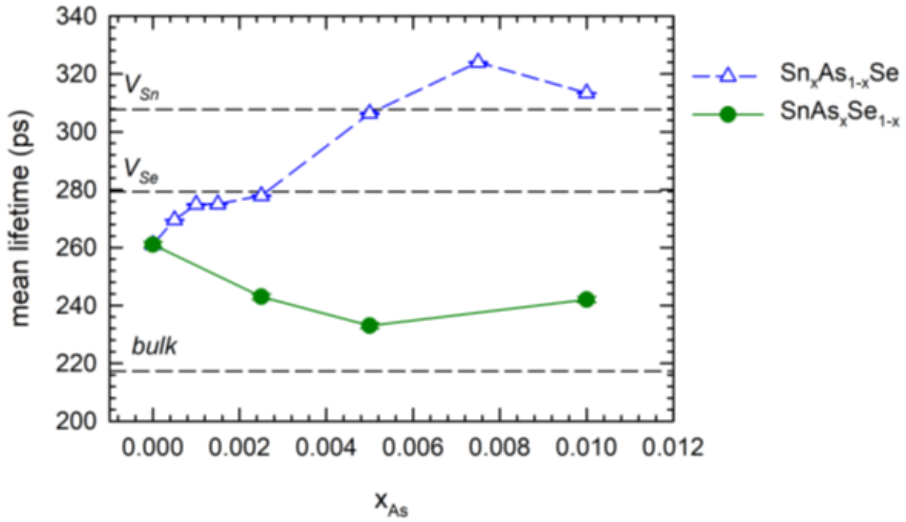

Fig 13. The mean positron lifetime τ_{mean} plotted as a function of the concentration x of As dopant in $SnAs_xSe_{1-x}$ and $Sn_{1-x}As_xSe$. The dashed lines show the calculated positron lifetimes for a perfect SnSe lattice (bulk) and for intrinsic mono- vacancies V_{Se}, V_{Sn}.

Investigations of binary $Sn_{2-y}Se_y$ SCs confirmed that Sn-poor conditions lead to formation of V_{Sn}. Similar effect occurs also in the $Sn_{1-x}As_xSe$, where some fraction of As dopants substitute Se ions instead of Sn ones leading to stoichiometric shift (Sn deficiency) due to As doping. In contrast to this in the $SnAs_xSe_{1-x}$, As dopants substitute almost exclusively Se ions and an unintentional shift in the stoichiometry plays a negligible role.

These conclusions are further supported by coincidence Doppler broadening (CDB). Fig. 15 presents CDB ratio curves related to the Al reference for $SnAs_xSe_{1-x}$ and $Sn_{1-x}As_xSe$. The CDB ratio curves of $SnAs_xSe_{1-x}$ samples increase in the high momentum range with increasing As concentration and exhibit growing contribution of positrons annihilated in the vicinity of As ions, see Fig. 15*a*. It indicates that the concentration of V_{Sn} decreases and that As ions are located preferentially in nearest neighbour sites around V_{Sn}. On the other hand, $Sn_{1-x}As_xSe$ samples exhibit opposite behaviour: the high momentum contribution decreases with increasing As concentration and the ratio curves become "Se-like" with a pronounced minimum at $p \approx 13\times10^{-3}$ m_0c, see Fig. 15*b*. It indicates increasing concentration of open volume defects, namely V_{Sn}, which are surrounded by Se ions in nearest neighbour sites. Hence, CDB results support the picture outlined by LT spectroscopy that $SnAs_xSe_{1-x}$ samples contain V_{Sn} associated

with As_{Se} nearest neighbours, and their concentration decreases with increasing As content, while $Sn_{1-x}As_xSe$ samples contain V_{Sn} that are not coupled with As, and their concentration increases with the As content.

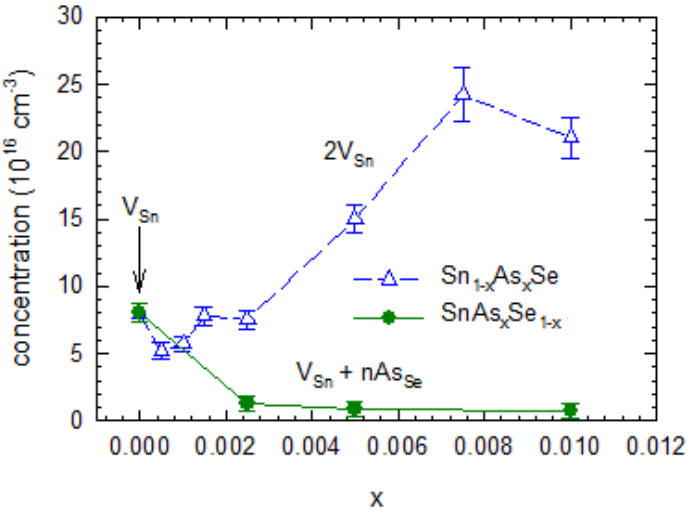

Fig 14. The concentrations of point defects detected by LT spectroscopy in As-doped SnSe SCs plotted as a function of As content, namely V_{Sn} for x = 0, V_{Sn} complexes with As_{Se} for the $SnAs_xSe_{1-x}$ (x > 0) and $2V_{Sn}$ for the $Sn_{1-x}As_xSe$ (x > 0)

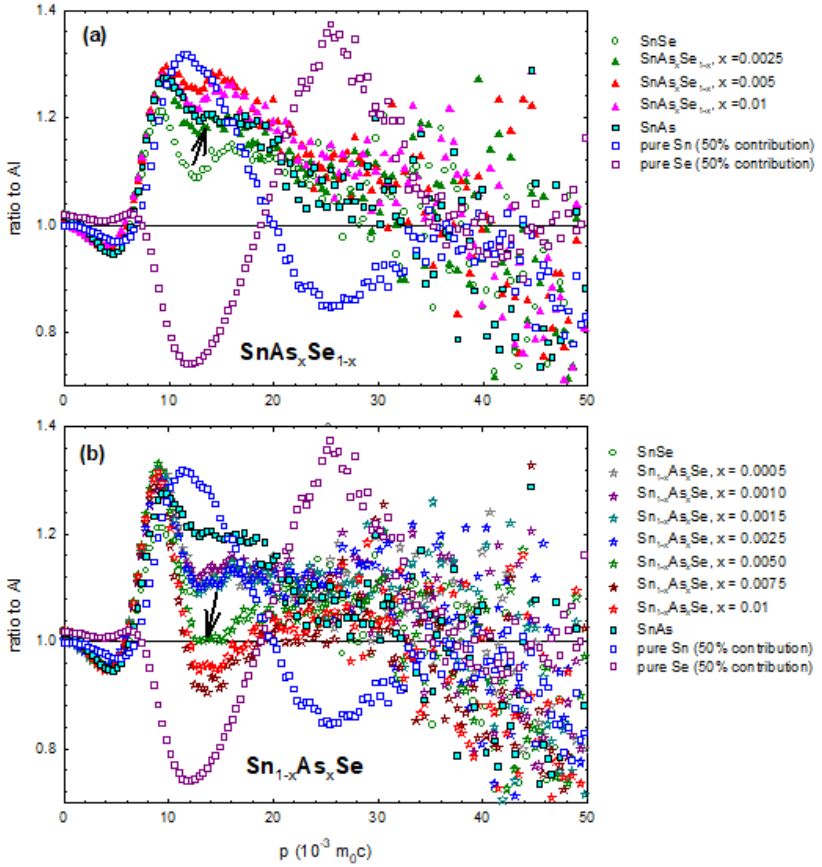

Fig 15. CDB ratio curves (related to Al) for (a) $SnAs_xSe_{1-x}$ samples and (b) $Sn_{1-x}As_xSe$ samples. The figure contains also CDB ratio curves for pure Sn and Se elements reduced to 50% contribution. The CDB ratio curve for SnAs compound is plotted in the figure as well. The arrows show the tendency upon doping.

5.3 Transport properties

The Hall concentration (HC) of holes decreases with As doping, reaching very low room temperature values, of the order of or even lower than 10^{16} cm^{-3} (x = 0.0075) for $Sn_{1-x}As_xSe$ (Fig. 16). In $Sn_{1-x}As_xSe$, there is a local minimum in the HC at approximately x = 0.001 due to the interaction of As_{Se} with V_{Sn}. First, the concentration of V_{Sn} generally decreases upon As doping (although the concentration of this defect increases due to the shift in stoichiometry for $x > 0.001$ in $Sn_{1-x}As_xSe$). This result is consistent with the conclusion drawn from PAS. Second, the activation energy of V_{Sn} (although not measured as discussed below) increases evidently due to coupling with As_{Se} defects. Namely, 1.7 V_{Sn} are needed to produce one hole in undoped SnSe, while more than 11 V_{Sn} are necessary for the same effect in $Sn_{1-x}As_xSe$ for x = 0.0075. Furthermore, a comparison of Figs. 15*a* and Fig. 16 implies that any higher concentration of V_{Sn} for $x > 0.001$ in $Sn_{1-x}As_xSe$ is not reflected in an associated increase in HC. The Hall coefficient is almost temperature independent for all the samples, although a very small activation appears for the undoped sample above 400 K that can be attributed to V_{Sn}.

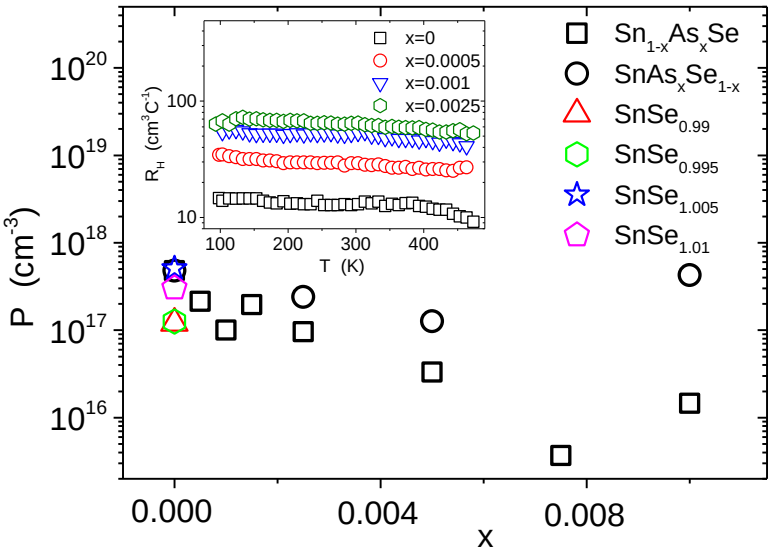

Fig. 16. The room temperature Hall concentration P for As-doped SnSe SCs as a function of the As content x, and non-stoichiometric $Sn_{2-y}Se_y$ SCs. The Hall concentration $P = 1/R_H e$, where R_H is the Hall coefficient and e is the electron charge. The inset shows the Hall coefficient as a function of temperature for the four lowest concentrations of As for $Sn_{1-x}As_xSe$. The Hall concentration of non-stoichiometric samples is provided for comparison.

It must be stressed that such a low concentration of holes as in the $Sn_{1-x}As_xSe$ for x = 0.0075 is not achieved in undoped SnSe samples by any other means. We observe the lowest concentration of holes of $\approx 2\times10^{17}$ cm^{-3} at room temperature (RT) in an undoped stoichiometric sample that was cooled down from melt to room temperatures over 8 weeks to reach the room temperature equilibrium state. Likewise, the same procedure including tuning the Sn/Se stoichiometry can decrease the RT concentration of holes to $\approx 8\times10^{16}$ cm^{-3} (for a composition of $SnSe_{0.99}$), which is connected with depletion of V_{Sn}.

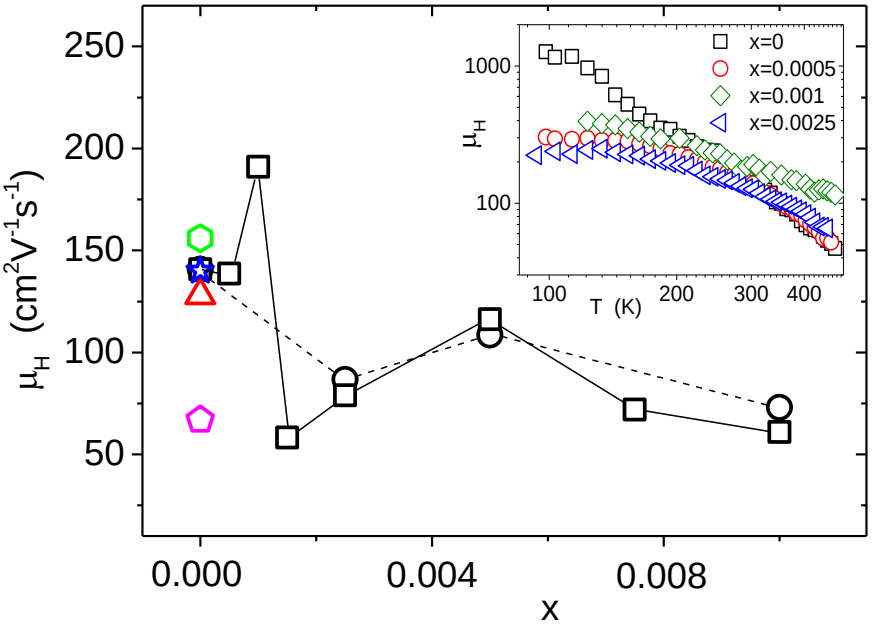

Fig. 17. The room temperature Hall mobility $\mu_H = R_H\sigma$ for As-doped SnSe SCs as a function of the As content, x. The Hall mobility of non-stoichiometric $Sn_{2-y}Se_y$ SCs is provided for comparison. Please use the legend of Fig. 16. The inset shows the Hall mobility as a function of temperature for the four lowest concentrations of As in $Sn_{1-x}As_xSe$.

Generally, As doping decreases the FC mobility, $\mu(T)$ (Fig. 17), indicating the embedding of As atoms into the SnSe matrix, i.e., formation of point substitutional defects of As in place of Se (As_{Se}). The mobility of the undoped sample is comparable with published data [28]. The decrease in the Hall mobility is more pronounced in the $Sn_{1-x}As_xSe$ for $x > 0.005$. This result is in accordance with conclusions drawn from PAS that the $Sn_{1-x}As_xSe$ contains a much higher concentration of Sn vacancies. On the other hand, the mobility difference is not dramatic, which suggests that the effective scattering cross-section of V_{Sn} is not large in comparison to As_{Se} (compare also with non-stoichiometric samples). In addition, As doping varies the scattering mechanism (inset of Fig. 17). While the $\mu(T)$ of the undoped sample follows scattering on acoustic phonons over the whole temperature range measured, the $\mu(T)$ of the As-doped samples indicates an admixture of other types of scattering on impurities (lower absolute slope in inset of Fig. 17) [29]. Thus, we observed an increase in the concentration of impurities, in accordance with PAS, but no increase in the FC concentration. This result implies that As_{Se} and the derived complexes are deep donors/acceptors with higher activation energy. Unfortunately, measurements at higher temperatures ($T > 500$ K) lead to hysteresis of the transport parameters upon temperature cycling, which interferes with the activation energy measurement. Note that although the FC mobility generally decreases upon As doping, this parameter exceeds the values for pure SnSe for $x \approx 0.001$ in the higher temperature region. Hence, the decrease in the scattering magnitude of native defects more than compensates for the increase in scattering due to As_{Se} defects in this case. This result suggests a healing process. This result could be important for optical or photovoltaic (PV) applications, where the native defects are related to nonstoichiometry and hence formation of extraneous phases that are detrimental to the efficiency of PV conversion [30]. Although the Hall mobility μ_H can differ markedly

from the drift mobility μ for different Fermi levels or varying scattering mechanisms [31], the healing process is indisputable [32].

Conclusion

The study showed that single-crystalline SnSe in an equilibrium-close state has a pronounced defect structure at all temperatures that is governed by vacancies. Tin vacancies V_{Sn} dominate at low temperatures ($T \leq 500$ K), while selenium vacancies V_{Se} and clusters $V_{Sn} + nV_{Se}$ dominate at higher temperatures. This implies that SnSe prefers a Se-rich composition at low temperatures and a Se-poor composition at higher temperatures ($T \geq 600$ K), i.e., its actual stoichiometry varies with temperature.

The occurrence of V_{Se} and clusters $V_{Sn} + nV_{Se}$ is connected with an increase in the DOS effective mass. This increase could be real or virtual. Namely, it can be induced by a shift of the scattering mechanism of FCs towards a more energetically dependent mechanism, which is connected with a higher Seebeck coefficient, than for scattering by acoustic phonons for the same FC concentration. Hence, a virtually larger DOS effective mass of FCs is obtained. The occurrence of V_{Se} and vacancy clusters might be the reason for this phenomenon.

We suggest an explanation for why the TE properties of SCs are always much better than the TE properties of PCs. We hypothesize that the concentration of defects remains much higher in SCs than in PCs. The reason might be that such defects (being created due to the variation in the equilibrium stoichiometry with temperature) can accumulate at grain boundaries in PC while staying within the bulk in SC. The defects formed within the SC bulk keep their nanoscopic nature; hence, they can dissolve and precipitate upon cycling repeatedly.

In the As doping study on polycrystals it has been found that in both studied systems, the As-atoms interact with intrinsic defects in SnSe and very effectively suppress the formation of the V_{Sn}^{2-}. A similar limited solubility of As was found in its substitution at the cation site (as well as the anion site). Here, one can conclude that As behaves as an amphoteric dopant, i.e. substitutes both for the cation (As_{Sn}^{+}) and the anion (As_{Se}^{-}), however, neither of the defects does not significantly contribute to the electronic transport. Moreover, the thermoelectric properties of the studied systems are affected by the formation of the secondary phases in the matrix compound. Thus, the thermoelectric efficiency is either not enhanced at all ($Sn_{1-x}As_xSe$) or it is enhanced only in the middle of the temperature range studied ($SnAs_xSe_{1-x}$).

The results of As doping study on single crystals can be summarized as follows. $SnAs_xSe_{1-x}$: As atoms tend to substitute preferentially for Se atoms. The concentration of V_{Sn} decreases with As content by an order of magnitude, and around 80 % of positrons annihilate in the free state for $x = 0.01$, indicating that As increases the formation energy of V_{Sn}. The remaining small number of V_{Sn} are preferentially coordinated with As atoms. Importantly, the Hall concentration decreases upon doping. A slight As substitution for Se clearly leads to healing of the host structure due to the removal of Sn vacancies. The As-induced depletion of extraneous phase $SnSe_2$ is corroborated by the HRXRD results. However, the carrier mobility tends to decrease with As doping, generally indicating a structural disorder due to As substitution.

$Sn_{1-x}As_xSe$: In contrast to the previous series, the concentration of V_{Sn} markedly increases with As content, and the vacancies are coordinated preferentially with Se. The

annihilation of positrons with As electrons is less evident, suggesting that As atoms partially coordinate with Sn vacancies only in the $SnAs_xSe_{1-x}$. As_{Se} is a deep defect that produces no FCs at room temperature. Correspondingly, the Hall concentration decreases upon doping and stays below 10^{16} cm^{-3} for $x = 0.0075$.

From the study of As-doped single crystals it follows, that doping of SnSe is a rather complex process that generally includes a strong interaction of doping atoms with the hosting structure. Such a strong interaction, on the other hand, indicates that doping could generally be used to adjust the type and concentration of defects. From this perspective, a high concentration of V_{Sn} or vacancy cluster defects might enable low-temperature TE application of SnSe. In terms of defect structure healing, further exploration of SnSe for photovoltaic applications is also worthwhile. However, the diverse interactions of defects with doping species that are temperature-dependent generally impede any high-temperature applications of SnSe.

List of references

[1] Nolas G. S., Sharp J., and Goldsmid H. J., *Thermoelectrics, Basic Principles and New Materials Developments* (Springer, Berlin, 2001), ISBN 978-3-540-41245-8.

[2] Zhao L.-D., Lo S.-H., Zhang Y., Sun H., Tan G., Uher C., Wolverton C., Dravid V. P., and Kanatzidis M. G., Ultralow thermal conductivity and high thermoelectric figure of merit in SnSe crystals. *Nature* (London) **508**, 373-377 (2014).

[3] Sassi S., Candolfi C., Vaney J.B., Ohorodniichuk V., Masschelein P., Dauscher A., and Lenoir B., Assessment of the thermoelectric performance of polycrystalline p-type SnSe. *Appl. Phys. Lett.* **104**, 212105 (2014).

[4] Chen Ch.-L., Wang H., Chen Y.-Y., Day T., and Snyder G. J., Thermoelectric properties of p-type polycrystalline SnSe doped with Ag. *J. Mater. Chem. A.* **2**, 11171-11176 (2014).

[5] Dewandre A., Hellman O., Bhattacharya S., Romero A. H., Madsen G. K. H., and Verstraete M. J., Two-Step Phase Transition in SnSe nad the Origins of Its High Power Factor from First Principles, *Phys. Rev. Lett*. **117**, 276601 (2016).

[6] Wei W., Chang Ch., Yang T., Liu J., Tang H., Zhang J., Li Y., Xu F., Zhang Z., Li J. F., and Tang G., Achieving high thermoelectric figure of merit in polycrystalline SnSe via introducing Sn vacancies, *J. Am. Chem. Soc.* **140**, 499 (2018).

[7] Wu D., Wu L., He D., Zhao L.-D., Li W., Wu M., Jin M., Xu J., Jiang J., Huang L., Zhu Y., Kanatzidis M. G., and He J., Direct observation of vast off-stoichiometric defects in single crystalline SnSe, *Nano Energy*. **35**, 321-330 (2017).

[8] Huang Y., Wang Ch., Chen X., Zhou D., Du J., Wang S., and Ning L., First-principles study on intrinsic defects of SnSe, *RSC Adv.* **7**, 27612 (2017).

[9] Duvjir G., Min T., Ly T. T., Kim T., Duong A.-T., Cho S., Rhim S. H., Lee J., and Kim J., Origin of p-type characteristics in a SnSe single crystal, *Appl. Phys. Lett*. **110**, 262106 (2017).

[10] Sist M., Zhang J., and Brummerstedt Iversen B., Crystal structure and phase transition of thermoelectric SnSe, Acta Crystallogr., Sect. B: Struct. Sci., Cryst. Eng. Mater. **72**, 310-316 (2016).

[11] Chattopadhyay T., Pannetier J., and Schnering H. G., Neutron diffraction study of the structural phase transition in SnS and SnSe. *J. Phys. Chem. Solids*. **47**, 879-885 (1986).
[12] Wang Z., Fan C., Shen Z., Hua Ch., Hu Q., Sheng F., Lu Y., Fang H., Qiu Z., Lu J., Liu Z., Liu W., Huang Y., Xu Z.-A., Shen D. W., and Zheng Y., Defects controlled hole doping and multivalley transport in SnSe single crystals, Nat. Commun. **9**, 47 (2018).
[13] Wei T.-R., Tan G., Zhang X., Wu Ch.-F., Li J.-F., Dravid V. P., Snyder G. J., and Kanatzidis M. G., Distinct Impact of Alkali-Ion Doping on Electrical Transport Properties of Thermoelectric p-Type Polycrystalline SnSe, *J. Am. Chem. Soc.* **138**, 8875-8882 (2016).
[14] Kucek V., Plechacek T., Janicek P., P Ruleova., Benes L., Navratil J., and Drasar C., Thermoelectric Properties of Tl-Doped SnSe: A Hint of Phononic Structure, *J. Electron. Mater.* **45**, 2943-2949 (2016).
[15] Shi X., Wu A., Fen T., Zheng K., Liu W., Sun Q., Hon M., Pantelides S. T., Chen Z.-G., and Zou J., High Thermoelectric Performance in p-type Polycrystalline Cd-doped SnSe Achieved by a Combination of Cation Vacancies and Localized Lattice Engineering, *Adv. Energy Mater.* 1803242 (2019).
[16] Yang J., Zhang G., Yang G., Wang Ch., and Wang Y. X., Outstanding thermoelectric performances for both p-and n-type SnSe from first-principles study, *J. Alloys Compd*. **644**, 615 (2015).
[17] Duong A. T., Nguyen V. Q., Duvjir G., Duong V. T., Kwon S., Song J. Y., Lee J. K., Lee J. E., Park S.D., Min T., Lee J., Kim J., and Cho S., Achieving ZT=2.2 with Bi-doped n-type SnSe single crystals, *Nat. Commun*. **7**, 13713 (2016).
[18] Li S., Wang Y., Chen Ch., Li X., Xue W., Wang X., Zhang Z., Cao F., Sui J., Liu X., and Zhang Q., Heavy Doping by Bromine to Improve the Thermoelectric Properties of n-type Polycrystalline SnSe, *Adv. Sci*. **5**, 1800598 (2018).
[19] https://www.ill.eu/sites/fullprof/.
[20] Krause-Rehberg R. and Leipner H., Positron Annihilation in Semiconductors (Springer-Verlag, Berlin, 1999).
[21] Asoka-Kumar P., Alatalo M., Ghosh V. J., Kruseman A. C., Nielsen B., and Lynn K. G., Increased Elemental Specificity of Positron Annihilation Spectra, *Phys. Rev. Lett*. **77**, 2097 (1996).
[22] Becvar F., Cizek J., Prochazka I., and Janotova J., The asset of ultra-fast digitizers for positron-lifetime spectroscopy, *Nucl. Instrum. Methods Phys. Res., Sect. A* **539**, 372 (2005).
[23] Prochazka I., Novotny I., and Becvar F., Application of maximum-likelihood method to decomposition of positronlifetime spectra to finite number of components, *Mater. Sci. Forum.* **255-257**, 772 (1997).
[24] Cizek J., Vlcek M., and Prochazka I., Digital spectrometer for coincidence measurement of Doppler broadening of positron annihilation radiation, *Nucl. Instrum. Methods Phys. Res., Sect. A* **623**, 982 (2010).
[25] Serrano-Sánchez F., Nemes N. M., Dura O. J., Fernandez-Diaz M. T., Martínez J. L., and Alonso J. A., Structural phase transition in polycrystalline SnSe: A neutron diffraction study in correlation with thermoelectric properties, *J. Appl. Cryst.* **49**, 2138 (2016).

[26] Cermak P., Ruleova P., Holy V., Prokleska J., Kucek V., Palka K., Benes L., and Drasar C., Thermoelectric and magnetic properties of Cr-doped single crystal Bi_2Se_3-Search for energy filtering, *J. Solid. State. Chem.* **258**, 768 (2018).
[27] Tang G.D., Wei W., Zhang J., Li Y.S., Wang X., Xu G.Z., Chang C., Wang Z.H., Du Y.W., Zhao L.D.: Realizing high figure of merit in phase-separated polycrystalline $Sn_{1-x}Pb_xSe$. *J. Am. Chem. Soc.* **138**, 13647–13654 (2016).
[28] Wang Z., Fan C., Shen Z., Hua Ch., Hu Q., Sheng F., Lu Y., Fang H., Qiu Z., Lu J., Liu Z., Liu W., Huang Y., Xu Z.-A., Shen D. W., and Zheng Y., Defects controlled hole doping and multivalley transport in SnSe single crystals, *Nat. Commun.* **9**, 47 (2018).
[29] Cermak P., Knotek P., Ruleova P., Holy V., Palka K., Kucek V., Benes L., Navratil J., and Drasar C., High power factor and mobility of single crystals of Bi_2Se_3 induced by Mo doping, *J. Solid State Chem.* **277**, 819 (2019).
[30] Burton L. A., Colombara D., Abellon R. D., Grozema F. C., Peter L. M., Savenije T. J., Dennler G., and Walsh A., Synthesis, Characterization, and Electronic Structure of Single-Crystal SnS, Sn_2S_3, and SnS_2, *Chem. Mater.* **25**, 4908 (2013).
[31] Fistul V. I., Heavily Doped Semiconductors (Springer, Boston, 1969), p.108-125.
[32] See suplementary material for Cermak Sraitrova K., Cizek J., Holy V., Plechacek T., Kucek V., Navratil J, Krejcova A., and Drasar C., As-doped SnSe single crystals: Ambivalent doping and interaction with intrinsic defects, *Phys. Rev. B.* **103**, 085203 (2021).

List of Students' Published Works

Impact Factor Journals

[1] Sraitrova K., Cizek J., Holy V., Plechacek T., Benes L., Jarosova M., Kucek V., and Drasar C., Vacancies in SnSe single crystals in a near-equilibrium state, *Phys. Rev. B.* **99**, 035306 (2019).
[2] Cermak Sraitrova K., Cizek J., Holy V., Plechacek T., Kucek V., Navratil J, Krejcova A., and Drasar C., As-doped SnSe single crystals: Ambivalent doping and interaction with intrinsic defects, *Phys. Rev. B.* **103**, 085203 (2021).

Non-Impact Peer-Reviewed Journals

[1] Navrátil J., Šraitrová K., Kucek V., Plecháček T., Kašparová J., and Drašar Č., Investigation of an amphoteric behaviour of arsenic dopant in polycrystalline SnSe, *Sci. Pap. Univ. Pardubice, Ser. A* **24**, 87 (2018).

Conference Proceedings

[1] Šraitrová K., Kucek V., Ruleová P., Plecháček T., and Drašar Č., Study on the thermoelectric properties of polycrystalline SnSe doped with As, In *Proceedings of the 5th International Conference on Chemical Technology*. Praha: Česká společnost průmyslové chemie, 2017. s. 287-291. ISBN 978-80-86238-62-3.

Conference Talks

[1] Šraitrová K., Elektřina přímo z tepla? Termoelektrické materiály – podstata a perspektivy, *Veletrh Věda Výzkum Inovace*, Brno (Czech Republic), 28. 2. – 2. 3. 2017, ISBN 978-80-906697-2-7.

[2] Šraitrová K., Čermák P., Kucek V, Drašar Č., Influence of the dimensions of the sample on the measurements of Hall and Seebeck coefficient, *Development of materials science in research and education*, Kežmarské Žľaby (Slovakia), 4. 9. – 8. 9. 2017, ISBN 978-80-89597-67-3.

[3] Sraitrova K., Kucek V., Drasar C., Influence of nonstoichiometry on thermoelectric properties of single crystalline SnSe, *6th International Conference on Chemical Technology*, Mikulov (Czech Republic), 16. 4. – 18. 4. 2018, ISBN 978-80-86238-83-8.

[4] Sraitrova K., Holy V., Kucek V., Drasar C., Native defects in SnSe and their temperature dependence, *37th International and 16th European Conference on Thermoelectrics*, Caen (France), 1. 7. – 5. 7. 2018.

[5] Sraitrova K., Kucek V., Cermak P., Drasar C., Effect of Tl doping on thermoelectric properties of SnSe single crystals, *Development of Materials Science in Research and Education*, Pavlov (Czech Republic), 3. 9. – 7. 9. 2018, ISBN 978-80-905962-8-3.

[6] Čermák P., Plecháček T., Hejtmánek J., Levinský P., Svoboda R., Zmrhalová Z., Pálka K., Beneš L., Šraitrová K., Drašar Č., Investigation of stability of Tl-doped SnS, *Development of Materials Science in Research and Education*, Pavlov (Czech Republic), 3. 9. – 7. 9. 2018, ISBN 978-80-905962-8-3.

[7] Sraitrova K., Kucek V., Plechacek T., Drasar C., Single crystalline SnSe doped with As and its interaction with native defects, *13th International Conference on Solid State Chemistry*, Pardubice (Czech Republic), 16. 9. – 21. 9. 2018, ISBN 978-80-7560-158-2.

[8] Sraitrova K., Cizek J., Drasar C., Vacancies in SnSe single crystals in a near-equilibrium state, *17th European Conference on Thermoelectrics*, Limassol (Cyprus), 23. 9. – 25. 9. 2019.

[9] Sraitrova K., Levinsky P., Hejtmanek J., Kucek V., Drasar C., Tl-doped SnSe single crystals, *17th European Conference on Thermoelectrics*, Limassol (Cyprus), 23. 9. – 25. 9. 2019.

Conference Posters

[1] Šraitrová K., Kucek V., Ruleová P., Plecháček T., Drašar Č., Study on the Thermoelectric Properties of Polycrystalline SnSe Doped with As, *5th International Conference on Chemical Technology*, Mikulov (Czech Republic), 10. 4. – 12. 4. 2017, ISBN 978-80-86238-62-3.

[2] Sraitrova K., Kucek V., Ruleova P., Plechacek T., Drasar C., The effect of arsenic doping on the thermoelectric properties of polycrystalline SnSe, *15th European Conference on Thermoelectrics*, Padova (Italy), 25. 9. – 27. 9. 2017.

[3] Sraitrova K., Kucek V., Drasar C., SnSe doped with Tl and its mechanical properties, *6th International Conference on Chemical Technology*, Mikulov (Czech Republic), 16. 4. – 18. 4. 2018, ISBN 978-80-86238-83-8.